Precipitation sequences during carburisation of Cr–Mo steel

J. M. Race and H. K. D. H. Bhadeshia

When Cr–Mo steel is joined to mild steel and the joint held at an elevated temperature the carbon tends to migrate from the mild steel to the Cr–Mo alloy. This migration is driven by the higher chemical potential of carbon in the mild steel, and leads to a steady accumulation of carbon in the Cr–Mo steel at the weld junction. The present work demonstrates that the carbon enrichment has a strong effect on the sequence of carbides that forms during aging, and the results are rationalised using thermodynamic phase stability calculations. Similar data are reported for other dissimilar metal joints. *MST/1611*

 Manuscript received 3 January 1992. *Dr Race is in the Department of Engineering Metallurgy, NEI Parsons Ltd, Newcastle upon Tyne. Dr Bhadeshia is in the Department of Materials Science and Metallurgy, University of Cambridge, Cambridge/JRDC.*

Introduction

Dissimilar metal joints are used extensively in the power generation industry in boiler tubing to accommodate changes in temperature, pressure, and corrosive conditions between different locations. Typical service conditions in power plant typically involve temperatures in the range 540–680°C, and there is no specific alloy that is suitable to serve over this entire range. Consequently, the steel offering the greatest economic advantage in a narrower temperature range is used, necessitating a gradual change in alloy chemistry towards more concentrated alloys as the service temperature increases. A typical sequence of materials might be as follows:[1] carbon steel → 1Cr–0·5Mo → 2·25Cr–1Mo → 9Cr–1Mo → 12Cr–1Mo → 316 austenitic stainless steel, in order of increasing service temperature. Thus, joints must be made between ferritic steels of differing alloy contents and between austenitic and ferritic steels.

Joints of this type are prone to failure, which can cause steam leakage and expensive shutdowns. A principal cause of failure is the migration of carbon, generally from the low alloy to the high alloy side of the weld. The diffusion occurs to some extent during post-weld heat treatment, but mostly during subsequent service at elevated temperatures. This results in an area on one side of the weld interface that is depleted in carbon and therefore weaker in terms of stress rupture. The other side is correspondingly enriched and there may be further detrimental effects on the mechanical properties as a consequence.

The partitioning of carbon occurs even when both sides of the weld have identical carbon concentrations, because the driving force for such migration is the difference in carbon chemical potential caused by the variation in the substitutional solute content across the junction. The problem is analogous to the classic experiment by Darken[2] in which a junction between steels containing different substitutional solute contents was heated into the austenite phase field to induce the uphill diffusion of carbon. The present study, however, deals with diffusion below the austenitisation temperature. The matrix is therefore ferritic and carbide precipitates may be present on either side of the junction.

Since the solubility of carbon in ferrite is extremely low, in practice the partitioning of carbon involves the dissolution of carbides on the low alloy side of the weld, and the precipitation of carbides on the high alloy side of the weld. The precipitation of carbides at temperatures typical of those where the steels enter service begins with the formation of cementite, followed by a number of alloy carbides as the system tends towards equilibrium. Such sequences have been the subject of many previous studies,[3–6] but the specific purpose of the present work was to examine how the influx of carbon influences the precipitation reactions. Information of this type is vital in two respects. First, the present authors are in the process of developing a quantitative model for carbon diffusion at dissimilar ferritic joints. The concentration of carbon in the ferrite in equilibrium with the carbide on either side depends on the nature of the carbide. Second, the nature of carbide precipitation is expected to influence the mechanical properties at the weld junction.

Experimental methods

WELD DESIGN

The joint between the mild steel and 2·25Cr–1Mo was made by welding two mild steel plates together using Metrode (tradename, Metrode Products Ltd, Chertsey) 2CrMoB-G electrodes. The chemical compositions are given in Table 1. Note that not only is the activity of carbon expected to be smaller on the chromium rich side of the junction, but the diffusion effects discussed below are expected to be exaggerated by the higher starting carbon concentration in the mild steel. The weld was made in five layers using three different gauges of electrode and a preheat and interpass temperature of 100°C as shown in Fig. 1. The weld was sectioned parallel to the fusion surface of the baseplate and the specimens were sealed in quartz tubes under a partial pressure of argon. Heat treatments were carried out at 700°C for various times between 16 and 2000 h.

TRANSMISSION ELECTRON MICROSCOPY

As discussed in detail in the following subsection, transmission electron microscopy (TEM) was used to identify individual carbides in the region of the weld near to the fusion line via electron diffraction patterns and energy

Table 1 Compositions of weld and mild steel parent plate, wt-%

C	Si	Mn	P	S	Cr	Mo	Ni	V
Mild steel								
0·23	0·26	0·77	0·011	0·016	0·037	0·015	0·017	0·00
2·25Cr–1Mo weld								
0·079	0·43	0·98	0·011	0·012	2·17	0·99	0·053	0·025

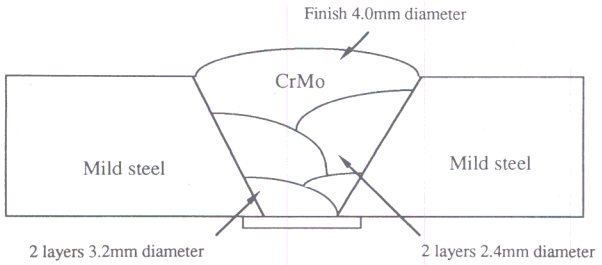

1 Welding sequence for mild steel/2·25Cr–1Mo joint

dispersive X-ray (EDX) microanalysis. For these identification techniques, carbon extraction replicas were used instead of thin foils to avoid spurious X-rays from the matrix.

The carbon replica extraction procedure developed by Smith and Nutting[7] was used to produce thin carbon films suitable for examination in the TEM. The metal surface was first polished and etched so that the structure was distinctly visible under the optical microscope. A thin carbon film was then evaporated onto the metal surface. The thin film was removed by etching in a solution of 5% chloral (hydrochloric acid in methanol) at a potential of 1·5 V until the film began to lift away from the surface. The specimen was then washed in alcohol before being transferred to a bath of distilled water where the replica was floated off and carefully collected on copper grids. The replicas were examined in the TEM using an accelerating voltage of 120 kV. The diffraction patterns were obtained using selected area apertures and chemical compositions were determined using EDX analysis with a specimen tilt of 35° towards the X-ray detector. A live time of 100 s was used, during which the dead time was not allowed to exceed 25%. The data were analysed using the Link RTS2 FLS programme for microanalysis, which corrects the data for atomic number and accounts for overlapping peaks by fitting to standard profiles.

IDENTIFICATION OF CARBIDES

Most of the carbide phases can, of course, be identified uniquely using electron diffraction, but this is in practice very difficult when examining large numbers of small particles. The carbides are often too thick or too thin to provide reasonable diffraction data, and the diffraction patterns can sometimes be ambiguous.

A frequently used alternative method in this type of research is based on EDX microanalysis. This technique for carbide identification is carried out in the TEM and permits chemical analyses to be taken from individual carbides. Pilling and Ridley[4] found that the carbides showed one of five characteristic X-ray spectra, as shown in Fig. 2. These spectra were identified using diffraction techniques and from the position and morphology of the carbides.

Thus, carbides in 2·25Cr–1Mo can now be identified using these spectra as standards. Titchmarsh[8] used a method based on EDX and diffraction patterns to produce some characteristic Mo/Cr and Fe/Cr count ratios which

Table 2 Mo/Cr and Fe/Cr count ratios for various carbides (From Ref. 8)

Precipitate	Mo/Cr count ratio	Fe/Cr count ratio
Mo_2C	2·0–4·0	0·05–0·10
Fe_3C	0·08–0·12	2·0–10·0
$M_{23}C_6$	0·05–0·10	0·50–0·70
M_6C	5·0–9·0	4·0–8·0
$M_{23}C_6$	0·15–0·20	1·1–1·4

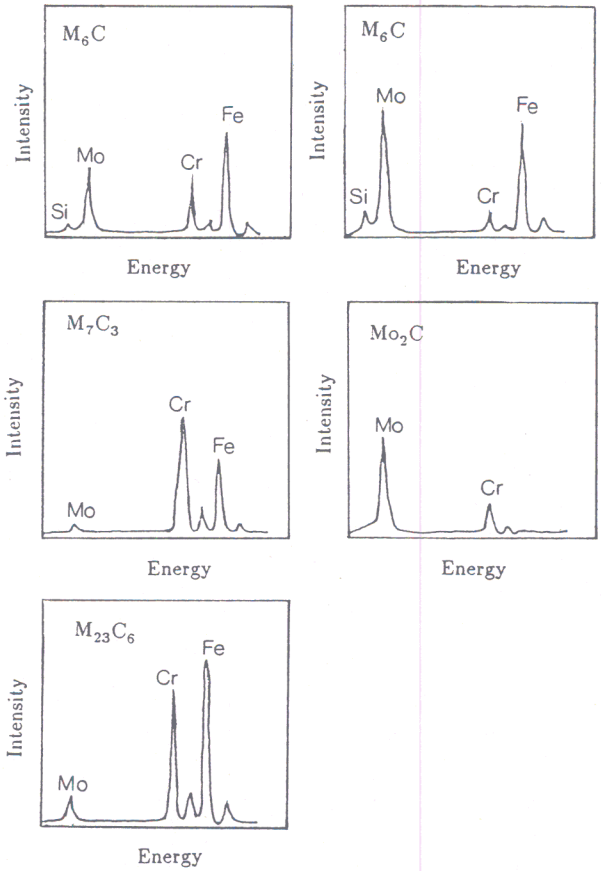

2 Characteristic X-ray spectra from various carbides (After Ref. 4)

also allow carbides to be identified rapidly. The results are given in Table 2.

Morphological differences can also act as a guide in the identification of carbides. Pilling and Ridley[4] suggest that there are four distinct carbide morphologies in specimens tempered at 700°C:

(i) globular precipitates at the prior austenite and lath grain boundaries
(ii) rodlike precipitates in the matrix
(iii) clusters of needle shaped precipitates in the matrix
(iv) parallelogram shaped particles in the matrix.

The distinctive needle shaped morphology is adopted by Mo_2C, and Pilling and Ridley[4] suggest that the grain boundary carbides are M_6C or $M_{23}C_6$ and that the rod shaped precipitates are M_7C_3. However, Balluffi *et al.*[9] have shown that $M_{23}C_6$ has a spherical form and Beech and Warrington[10] have shown that M_7C_3 and $M_{23}C_6$ have similar morphologies. Thus, it can be concluded that the shape of the particle alone is not a guide to identification.

All these methods, namely, electron diffraction, microanalysis, and morphological observations were used to identify the carbides.

Results and discussion

METALLOGRAPHY

A typical optical micrograph of the mild steel/2·25Cr–1Mo joint held at 700°C for 1024 h is shown in Fig. 3*a*.

The scanning electron micrographs (SEMs) in Figs. 3*b*–3*f* illustrate the change in carbide size and density across the welded joint. In the mild steel plate distant from the interface (Fig. 3*f*) the structure consists of grains of

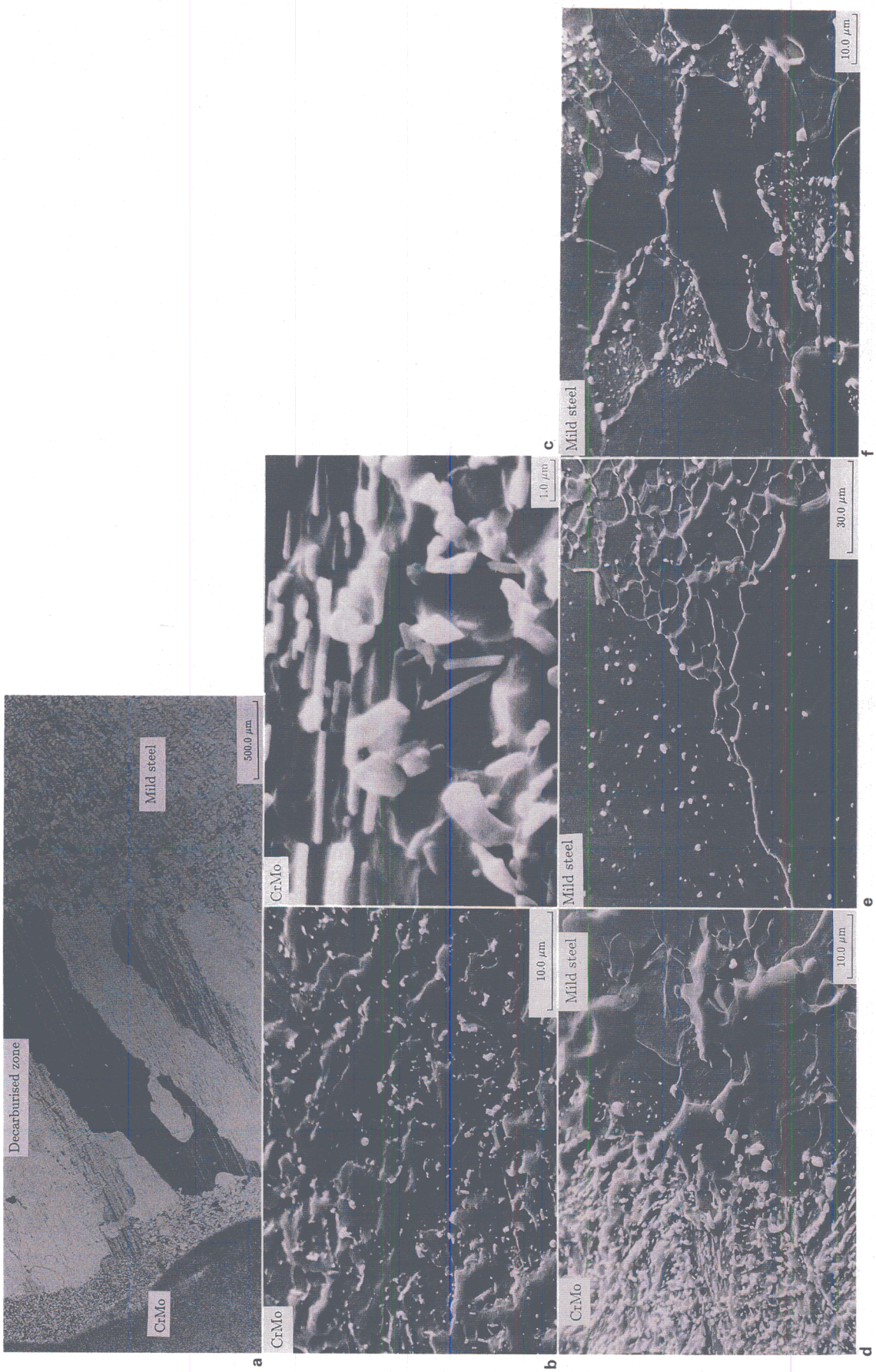

a complete weld region; *b* weld metal distant from interface; *c* carbides at interface; *d* interface; *e* decarburised zone; *f* parent plate
a optical micrograph; *b–f* SEM

3 Microstructure of mild steel/2·25Cr–1Mo weld heat treated at 700°C for 1024 h

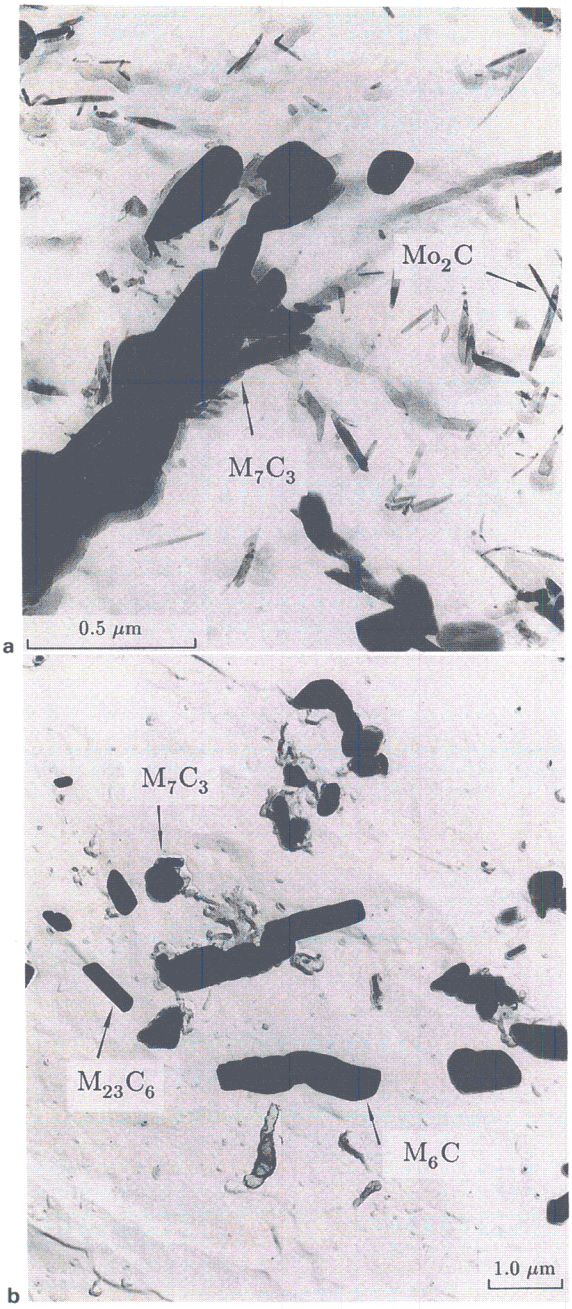

4 TEMs of region near interface in 2·25Cr–1Mo, showing morphology of carbide phases: carbides were identified using energy dispersive X-ray (EDX) analysis and diffraction patterns

ferrite and spheroidised pearlite. The decarburised zone is characterised by large grains of recrystallised ferrite which are free of carbides, thus allowing the grains to grow as the grain boundary pinning effect of the carbides is lost. The weld interface is very sharply defined by the large proportion of carbides found in the 2·25Cr–1Mo steel at the interface (Fig. 3*d*). If this is compared with the carbide density distant from the weld interface (Fig. 3*b*) it can be seen that there is increased carbide precipitation and growth of carbides at the interface (Fig. 3*c*).

The morphology of the carbide phases is more distinctly revealed using TEM. Typical micrographs are presented in Fig. 4. Whereas Mo_2C is readily identified by its needlelike morphology, the micrographs confirm that the other phases cannot be identified purely by their morphology.

	Fe_3C	Mo_2C	M_7C_3	$M_{23}C_6$	M_6C
16hours					
32 hours					
64 hours					
128 hours					
256 hours					
512 hours					
1024 hours					
2048 hours					

5 Carbides expected from work presented in Ref. 3

	Fe_3C	Mo_2C	M_7C_3	$M_{23}C_6$	M_6C
16hours		2	11		
32 hours			2	12	
64 hours		2	5	12	4
128 hours	15			6	
256 hours	2		2	11	
512 hours	12		3		
1024 hours	14			3	
2048 hours	5		3	8	4

6 Experimental results showing carbides found in present work (number of carbide particles measured is indicated in each box)

PRECIPITATION SEQUENCES

Baker and Nutting[3] conducted a classic study of carbide precipitation in 2·25Cr–1Mo steel as a function of time and tempering temperature. They suggested that the important phases precipitate in the following sequence:

$$\text{cementite} \rightarrow \begin{matrix}\text{cementite} \\ + \\ Mo_2C\end{matrix} \rightarrow M_{23}C_6 \rightarrow M_6C_3 \qquad \text{cementite} \rightarrow Cr_7C_3 \rightarrow M_6C_3$$

In practice, cementite dissolves fairly rapidly at 700°C, as illustrated by a selection of the data of Baker and Nutting[3] relevant to this work, which is presented in Fig. 5.

The results obtained in the present work are shown in Fig. 6. A comparison with the data of Baker and Nutting reveals large discrepancies, especially after prolonged aging.

The reappearance of cementite at the longer aging times indicates that the discrepancies may be attributed to the

Table 3 Equilibrium compositions (wt-%) of carbides found in 2·25Cr–1Mo calculated using Mtdata

Carbide	Fe	Cr	Mn	Mo	C
M_6C	27·93	38·92	0·001	19·468	2·50
M_7C_3	31·58	44·93	11·37	3·48	8·61
$M_{23}C_6$	58·68	20·22	0·003	16·08	5·04
Fe_3C	64·15	18·00	10·82	0·22	6·78

Table 4 Composition of weld and 12Cr–1Mo parent plate, wt-%

C	Si	Mn	P	S	Cr	Mo	Ni	V
12Cr–1Mo								
0·20	0·37	0·58	0·035	0·003	11·5	0·92	0·74	0·31
2·25Cr–1Mo weld								
0·08	0·43	1·01	0·011	0·003	2·42	1·00	0·064	0·028

carbon enrichment caused by diffusion through the dissimilar metal junction. This hypothesis was verified using thermodynamic phase calculations in which the carbon concentration of the 2·25Cr–1Mo steel was permitted to increase. These calculations were carried out using Mtdata,[11] which is a computer program and thermodynamic database for phase diagram computation. The phase calculations were carried out taking into account iron, chromium, molybdenum, manganese, carbon, silicon, nickel, vanadium, sulphur, and phosphorus as alloying elements, and ferrite, cementite, M_7C_3, M_6C, and $M_{23}C_6$ as the permitted phases at 700°C. The equilibrium chemical compositions of these carbides are given in Table 3, and the predicted equilibrium carbides are shown as a function of bulk carbon content in Fig. 7.

It is evident from Fig. 7 that the experimental results can be interpreted in terms of carbon enrichment. Furthermore, they demonstrate that the carbon concentration in the enriched zone must exceed 0·56 wt-% after 128 h at 700°C. Thus, comparing the experimental carbide results with those of Baker and Nutting and those predicted using Mtdata, it can be seen that in dissimilar metal welds, the diffusion of carbon from the low alloy side of the weld causes the normal precipitation sequence to be modified. The difference is accounted for by the increase in the local bulk carbon concentration.

Other steels

12Cr–1Mo/2·25Cr–1Mo WELD

This weld was made between a 12Cr–1Mo steel pipe and a 2·25Cr–1Mo pipe using 2·25Cr–1Mo electrodes, the compositions of which are given in Table 4. The weld preparation is shown in Fig. 8 and the weld was completed in 61 runs using a preheat of 100°C and an interpass temperature of 250°C.

	Fe_3C	Mo_2C	M_7C_3	$M_{23}C_6$	M_6C
0.1 wt% C				0.0214	0.00155
0.12 wt% C				0.0226	0.00035
0.13 wt% C				0.0286	
0.27 wt% C				0.0593	
0.28 wt% C			0.00367	0.0598	
0.55 wt% C			0.0286	0.0709	
0.56 wt%C	0.00245		0.0275	0.0712	
0.57 wt% C	0.00495		0.0294	0.0714	

7 Equilibrium carbides expected as function of bulk carbon concentration predicted using Mtdata: numbers in boxes indicate equilibrium volume fraction of each phase

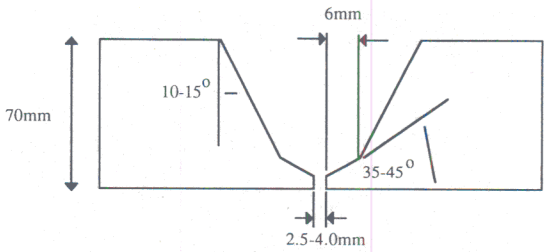

8 Preparation of 12Cr–1Mo/2·25Cr–1Mo weld

The diffusion was therefore from the 2·25Cr–1Mo weld into the 12Cr–1Mo parent, so decarburisation occurred in the weld metal and not the parent plate as in the previous experimental joint. A typical microstructure is shown in Fig. 9.

Carbide extraction replicas were taken from the 12Cr–1Mo side of the interface and analysed to determine the type of carbides precipitating during heat treatment. As can be seen from the sequence of TEMs presented in Fig. 10, there is a slight increase in carbide size and density with increasing aging time at 730°C, but no change in carbide type was found and the structure remained as $M_{23}C_6$ in ferrite on both sides of the 12Cr–1Mo/2·25Cr–1Mo weld junction.

Mtdata calculations (Fig. 11) are found to predict that it would be necessary for the bulk concentration at the interface to increase to about 3·0 wt-% to reprecipitate cementite, so it is not surprising that the carbide phase remained as $M_{23}C_6$ throughout the heat treatment.

Implications

The results presented above can be interpreted to provide an explanation of the extent of carbon diffusion which is observed in dissimilar ferritic joints. It might be expected that the degree of diffusion and therefore the width of the decarburised zone would be greatest in the 12Cr–1Mo/2·25Cr–1Mo joint owing to the greater difference in chromium concentration in this joint. However, this is not observed, as can be seen from the experimental evidence presented in Fig. 12.

In fact, it is the carbides present on either side of the interface that partly determine the extent of carbon diffusion. Consider the concentration gradients in the joint at the interface as illustrated in Fig. 13, where $x_{\alpha\beta}$ is the carbon concentration in the low alloy side at the weld interface (α), $x_{\beta\alpha}$ is the carbon concentration in the

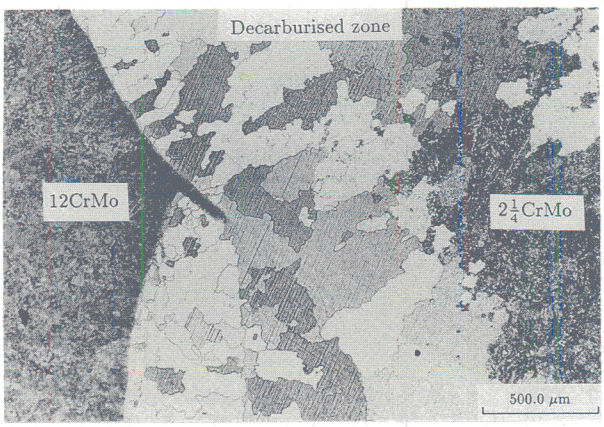

9 Decarburised zone in 12Cr–1Mo/2·25Cr–1Mo weld held for 64 h at 730°C (optical)

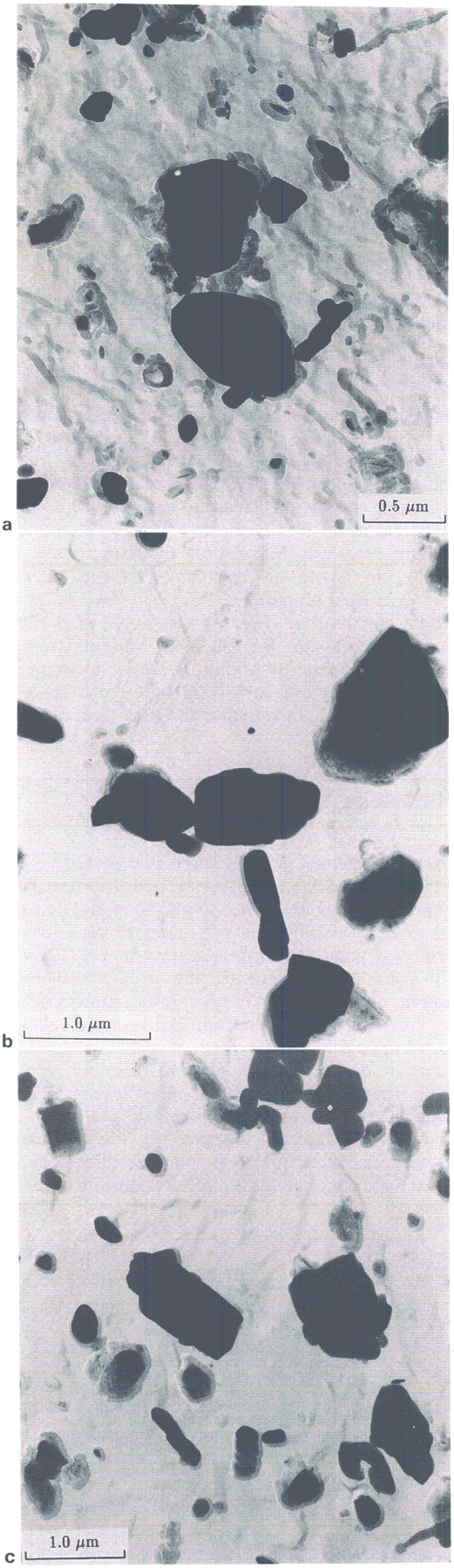

10 TEMs of 12Cr–1Mo at interface in weld held for *a* 16, *b* 256, and *c* 2048 h: carbide in all micrographs is $M_{23}C_6$, which was identified using EDX and diffraction techniques

	Fe_3C	Mo_2C	M_7C_3	$M_{23}C_6$	M_6C
0.2 wt% C			0.0251		
0.4wt% C				0.0837	
0.6 wt% C			0.0286	0.0777	
3.0 wt% C	0.1631		0.1824	0.0882	

11 Mtdata calculations showing carbide phases forming in 12Cr–1Mo with increasing carbon concentration at 730°C: numbers in boxes indicate equilibrium volume fractions of each phase

high alloy side at the weld interface (β), $x_{\alpha A}$ is the carbon concentration in the α ferrite in equilibrium with the carbide phase A, and $x_{\beta B}$ is the carbon concentration in the β ferrite in equilibrium with the carbide phase B.

The concentrations $x_{\alpha A}$ and $x_{\beta B}$ can of course be calculated thermodynamically, but the estimation of $x_{\alpha\beta}$ and $x_{\beta\alpha}$ requires some further discussion.

DETERMINATION OF INTERFACIAL COMPOSITIONS $x_{\alpha\beta}$ and $x_{\beta\alpha}$

Carbon diffusion at dissimilar metal joints can be described in terms of Laplace solutions for Fick's second law to determine a concentration profile, i.e.

$$x_\alpha = A_1 + B_1 \operatorname{erf}\left[\frac{z}{2(D_\alpha t)^{1/2}}\right] \quad \ldots\ldots\ldots \quad (1)$$

$$x_\beta = A_2 + B_2 \operatorname{erf}\left[\frac{|z|}{2(D_\beta t)^{1/2}}\right] \quad \ldots\ldots\ldots \quad (2)$$

where x_α and x_β are the concentrations of carbon in α and β, respectively at some distance z from the interface after time t, D_α and D_β are the diffusion coefficients of carbon in α and β ferrite, respectively, and A_1, B_1, A_2, and B_2 are constants determined from the boundary conditions. The boundary conditions for this situation are as follows.

1. There must be continuity of chemical potential μ across the interface, so that

$$\mu_{\alpha\beta} = \mu_{\beta\alpha} \quad \ldots\ldots\ldots\ldots\ldots\ldots \quad (3)$$

where the subscripts $\alpha\beta$ and $\beta\alpha$ denote the low and high alloy sides, respectively at the interface.

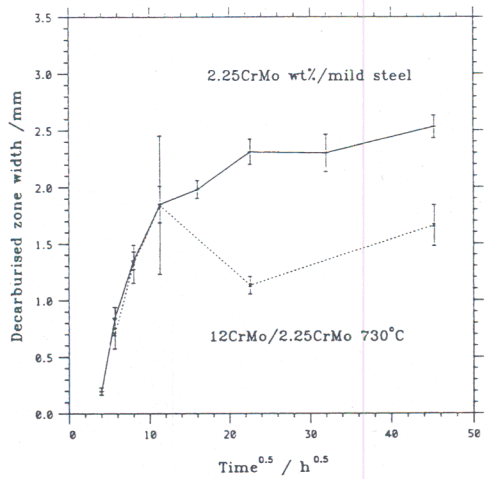

12 Decarburised zone width versus square root of time for mild steel/2·25Cr–1Mo and 12Cr–1Mo/2·25Cr–1Mo welds

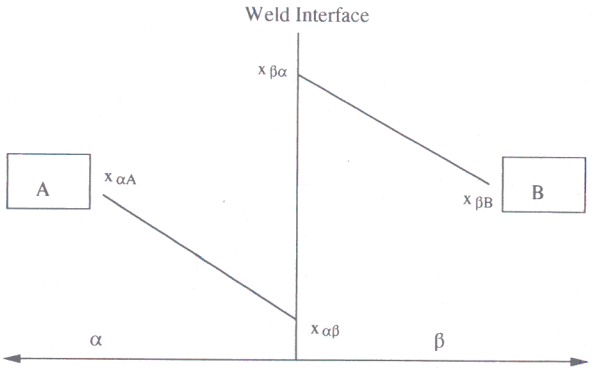

13 Schematic diagram of interfacial carbon concentrations: A and B are carbides and α and β are corresponding ferrite matrixes having different substitutional solute concentrations

2. There must be a continuity of flux across the interface, i.e. the carbon leaving one side must be equal to that entering the other side. It follows that

$$D\left.\frac{\partial x_\alpha}{\partial z}\right|_{z=0} = -D\left.\frac{\partial x_\beta}{\partial z}\right|_{z=0} \quad \ldots\ldots\ldots\ldots (4)$$

By application of these two boundary conditions, an expression for the constant A_1 can be derived as follows

$$A_1 = \frac{x_{\beta 0} + x_{\alpha 0}}{k+1} = x_{\alpha\beta} \quad \ldots\ldots\ldots\ldots (5)$$

where $x_{\alpha 0}$ and $x_{\beta 0}$ are the initial carbon concentrations in α and β, respectively and k is the partition coefficient, given by

$$k = \frac{x_{\beta\alpha}}{x_{\alpha\beta}} = \frac{\Gamma_\alpha}{\Gamma_\beta} \quad \ldots\ldots\ldots\ldots\ldots (6)$$

where Γ_α and Γ_β are the activity coefficients of carbon in α and β, respectively. The thermodynamic data of Wada *et al.*[12] were used to estimate the activity coefficients. Therefore, $x_{\alpha\beta}$ and $x_{\beta\alpha}$ can be determined by combination of equations (5) and (6).

If the appropriate values are used for a mild steel/2·25Cr–1Mo joint assuming that $M_{23}C_6$ is the dominant carbide at 700°C in 2·25Cr–1Mo and Fe_3C is the carbide in mild steel then the upper profile in Fig. 14 is obtained. Similarly, the values for a 12Cr–1Mo/2·25Cr–1Mo joint assuming $M_{23}C_6$ is the precipitate on both sides of the weld produce the lower profile in Fig. 14. This demonstrates that when the carbide phase is the same on either side of the interface, the gradients are much shallower so the driving force for diffusion is reduced.

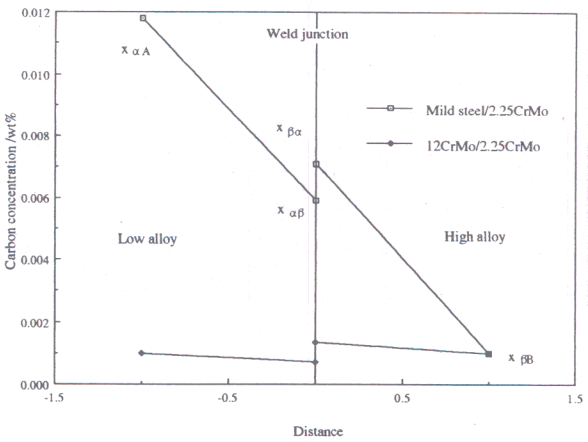

14 Calculated composition profiles for mild steel/2·25Cr–1Mo and 12Cr–1Mo/2·25Cr–1Mo welds

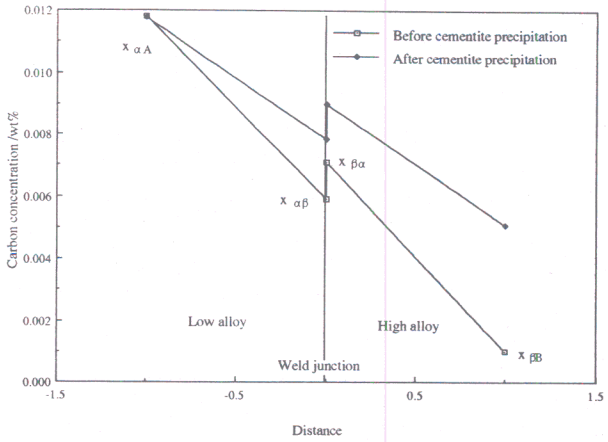

15 Calculated composition profiles for mild steel/2·25Cr–1Mo weld before and after cementite precipitation

Therefore, the mild steel/2·25Cr–1Mo weld is indeed expected to be more strongly decarburised than the 12Cr–1Mo/2·25Cr–1Mo weld.

A further implication results from the observation in Fig. 12 that the decarburised zone width tends to change at a decreasing rate when plotted against the square root of time. Classical diffusion theory would predict that this plot should be linear. This can be explained qualitatively by considering the effect on the gradients of the reprecipitation of cementite (Fig. 15). It can be seen that the profiles become less steep after cementite precipitation and therefore it would be expected that the rate of diffusion or the width of the decarburised zone would also tend to change at a slower rate, as observed experimentally.

Similarly, for the 12Cr–1Mo/2·25Cr–1Mo joint, although there is no change in carbide type, the value of $x_{\beta B}$ increases with carbon concentration (Fig. 16), therefore causing the profiles to become less steep at longer aging times.

Conclusions

The diffusion of carbon, as driven by the difference in its chemical potential on either side of a dissimilar metal ferritic joint, leads to radical changes in the carbide precipitation behaviour. The changes can however be predicted thermodynamically when the carbon enrichment is taken into account. The implications of this are significant, in that the reformation of cementite at long aging times will tend to reduce the rate of carburisation.

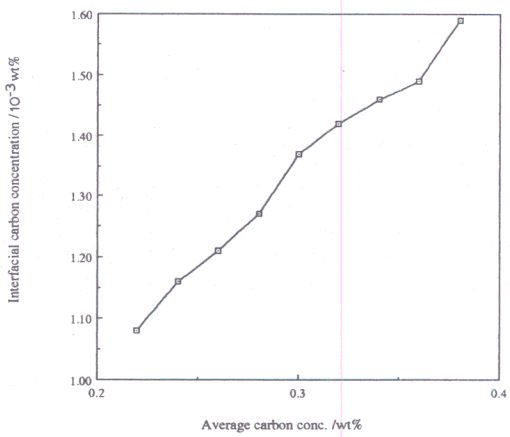

16 Variation of $x_{\beta B}$ with average carbon concentration for 12Cr–1Mo steel

Acknowledgments

The authors are grateful to Professor C. J. Humphreys for the provision of laboratory facilities at the University of Cambridge. The contribution of HKDHB to this work was carried out under the auspices of the 'Atomic arrangements: design and control' project, which is a collaboration between the University of Cambridge and the Research and Development Corporation of Japan (JRDC). The work of JMR was funded by NEI Parsons Ltd, Newcastle upon Tyne.

References

1. O. K. GORTON: in 'Materials in power plant' (Proc. Spring Meeting), Series 3, Vol. 3; 1975, London, The Institution of Metallurgists.
2. L. S. DARKEN: *Trans. AIME*, 1949, **180**, 430–438.
3. R. G. BAKER and J. NUTTING: *J. Iron Steel Inst.*, 1959, **192**, 257–268.
4. J. PILLING and N. RIDLEY: *Metall. Trans.*, 1982, **13A**, 557–563.
5. R. L. KLUEH and J. M. LEITNAKER: *Metall. Trans.*, 1975, **6A**, 2089–2093.
6. J. YU: *Metall. Trans.*, 1989, **20A**, 1561–1564.
7. E. SMITH and J. NUTTING: *J. Iron Steel Inst.*, 1957, **187**, 314–329.
8. J. M. TITCHMARSH: in Proc. 9th Int. Congress on 'Electron microscopy', (ed. J. M. Sturgess), Vol. I, 618–619; 1978, Toronto, ON, The Microscopical Society of Canada.
9. R. W. BALLUFFI, M. COHEN, and B. L. AVERBACH: *Trans. ASM*, 1951, **43**, 497–526.
10. J. BEECH and D. H. WARRINGTON: *J. Iron Steel Inst.*, 1966, **204**, 460–468.
11. Metallurgical and Thermochemical Databank (Mtdata), National Physical Laboratory, Teddington.
12. T. WADA, H. WADA, J. F. ELLIOTT, and J. CHIPMAN: *Metall. Trans.*, 1972, **3**, 2865–2872.